

# Atom-specific activation in CO oxidation

Cite as: J. Chem. Phys. **149**, 234707 (2018); <https://doi.org/10.1063/1.5044579>

Submitted: 14 June 2018 . Accepted: 08 October 2018 . Published Online: 21 December 2018

Simon Schreck, Elias Diesen, Jerry LaRue , Hirohito Ogasawara , Kess Marks , Dennis Nordlund, Matthew Weston, Martin Beye , Filippo Cavalca, Fivos Perakis , Jonas Sellberg , André Eilert, Kyung Hwan Kim, Giacomo Coslovich, Ryan Coffee , Jacek Krzywinski, Alex Reid , Stefan Moeller , Alberto Lutman, Henrik Öström, Lars G. M. Pettersson , and Anders Nilsson



View Online



Export Citation



CrossMark

## ARTICLES YOU MAY BE INTERESTED IN

[Ab initio investigation of magnetic anisotropy in intermediate spin iron\(iii\) complexes](#)

The Journal of Chemical Physics **149**, 234302 (2018); <https://doi.org/10.1063/1.5050037>

[Communication: Water activation and splitting by single metal-atom anions](#)

The Journal of Chemical Physics **149**, 221101 (2018); <https://doi.org/10.1063/1.5050913>

[Coulomb explosion imaging of CH<sub>3</sub>I and CH<sub>2</sub>ClI photodissociation dynamics](#)

The Journal of Chemical Physics **149**, 204313 (2018); <https://doi.org/10.1063/1.5041381>

PHYSICS TODAY

WHITEPAPERS

ADVANCED LIGHT CURE ADHESIVES

Take a closer look at what these environmentally friendly adhesive systems can do

READ NOW

PRESENTED BY  
 MASTERBOND  
ADHESIVES | SEALANTS | COATINGS



## Atom-specific activation in CO oxidation

Simon Schreck,<sup>1</sup> Elias Diesen,<sup>1</sup> Jerry LaRue,<sup>2</sup> Hirohito Ogasawara,<sup>3</sup> Kess Marks,<sup>1</sup> Dennis Nordlund,<sup>3</sup> Matthew Weston,<sup>1</sup> Martin Beye,<sup>4</sup> Filippo Cavalca,<sup>1</sup> Fivos Perakis,<sup>1</sup> Jonas Sellberg,<sup>5</sup> André Eilert,<sup>1</sup> Kyung Hwan Kim,<sup>1</sup> Giacomo Coslovich,<sup>3</sup> Ryan Coffee,<sup>3</sup> Jacek Krzywinski,<sup>3</sup> Alex Reid,<sup>3</sup> Stefan Moeller,<sup>3</sup> Alberto Lutman,<sup>3</sup> Henrik Öström,<sup>1</sup> Lars G. M. Pettersson,<sup>1</sup> and Anders Nilsson<sup>1,a)</sup>

<sup>1</sup>Department of Physics, AlbaNova University Center, Stockholm University, Stockholm SE-10691, Sweden

<sup>2</sup>Schmid College of Science and Technology, Chapman University, Orange, California 92866, USA

<sup>3</sup>SLAC National Accelerator Laboratory, 2575 Sand Hill Road, Menlo Park, California 94025, USA

<sup>4</sup>DESY Photon Science, Notkestrasse 85, Hamburg 22607, Germany

<sup>5</sup>Biomedical and X-ray Physics, Department of Applied Physics, AlbaNova University Center, KTH Royal Institute of Technology, SE-10691 Stockholm, Sweden

(Received 14 June 2018; accepted 8 October 2018; published online 21 December 2018)

We report on atom-specific activation of CO oxidation on Ru(0001) via resonant X-ray excitation. We show that resonant 1s core-level excitation of atomically adsorbed oxygen in the co-adsorbed phase of CO and oxygen directly drives CO oxidation. We separate this direct resonant channel from indirectly driven oxidation via X-ray induced substrate heating. Based on density functional theory calculations, we identify the valence-excited state created by the Auger decay as the driving electronic state for direct CO oxidation. We utilized the fresh-slice multi-pulse mode at the Linac Coherent Light Source that provided time-overlapped and 30 fs delayed pairs of soft X-ray pulses and discuss the prospects of femtosecond X-ray pump X-ray spectroscopy probe, as well as X-ray two-pulse correlation measurements for fundamental investigations of chemical reactions via selective X-ray excitation. *Published by AIP Publishing.* <https://doi.org/10.1063/1.5044579>

### I. INTRODUCTION

Even the most selective materials for catalyzing thermally driven reactions are limited in terms of efficiency due to so-called volcano-type scaling relations. These scaling relations give the reaction yield as a function of a single descriptor which can be, e.g., the *d*-band center or an atomic binding energy.<sup>1–5</sup> They stem from a balance between bond strengths of reactants, intermediates, and products to the substrate, where the initial bond-breaking is favored by strong chemisorption of the reactants, while the product should desorb easily. In thermally driven heterogeneous catalysis, the available energy is distributed equally among all accessible degrees of freedom. The outcome of the reaction in terms of the product ratio is then determined by the relative heights of the free-energy barriers leading to different products. In a system with competing reaction channels, it is desirable to activate the system differently to favor the preferred product. This requires a selective excitation mechanism that is fundamentally different from thermal excitation.

On the path toward controlling chemical reactivity and breaking these volcano-type scaling relations, we need to increase our understanding of selective excitation and how it can control surface reactivity from a fundamental perspective. Along these lines, the field of surface photo- and femtochemistry has developed, where a wealth of adsorbate reactions on catalytic surfaces driven by (laser) light from the infrared

to the ultraviolet spectral region have been studied in great detail (see Refs. 6–8 and the references therein). In terms of controlling surface reactivity, direct and indirect electronic adsorbate excitations by the incident light have been of particular interest.<sup>9–13</sup> Furthermore, strong electric fields to manipulate surface adsorbates have been explored.<sup>14–16</sup> Recently, LaRue *et al.*<sup>17</sup> used intense, quasi-half-cycle THz pulses with an associated electric field of  $\sim 1$  V/nm to induce CO oxidation from co-adsorbed CO and oxygen on Ru(0001) without observing the otherwise competing CO desorption process. The use of X-rays to induce processes in surface adsorbate systems is studied intensively since the advent of synchrotron radiation (see Refs. 8, 18–20 and the references therein), focusing on desorption of adsorbate fragments and ions and selective dissociation. However, the associative chemical reaction yielding product AB from reactants A and B remained elusive.

Today, X-ray free-electron lasers (XFELs) produce high-intensity, few-femtosecond X-ray pulses. Novel XFEL schemes generate X-ray double pulses with gigawatt power and precisely controlled time delay and wavelength separation.<sup>21–25</sup> With these capabilities, we can aim at transferring established optical laser techniques, such as two-pulse correlation,<sup>7,26,27</sup> into the X-ray regime and study the dynamics of X-ray activated processes, such as formation of new chemical bonds. Furthermore, we can envision X-ray pump X-ray spectroscopy probe experiments with few femtosecond time resolution to monitor the valence electronic structure of adsorbates after selective activation by soft X-rays.<sup>28–31</sup>

<sup>a)</sup>andersn@fysik.su.se

In this work, we take a first step toward this vision and report on CO oxidation on Ru(0001) driven by resonant soft X-ray excitation. We use a single pulse as well as a sequence of two 30 fs delayed X-ray pulses (double pulse) of a few femtosecond duration at different intensities to drive CO oxidation. Using different photon energies, we show that  $1s$  core-level excitation of atomically adsorbed oxygen can directly induce CO oxidation in the co-adsorbed phase of CO and oxygen on Ru(0001). We separate the direct activation via core-level excitation of the adsorbate from the competing indirect activation that is driven via X-ray excitations in the substrate. Using density functional theory (DFT) calculations, we identify the valence-excited Auger final state of atomically adsorbed oxygen as the driving electronic state for CO oxidation. With the double-pulse photon energy tuned to the atomic oxygen resonance, we observe an enhanced contribution from indirect activation via the substrate to the total reaction yield which we tentatively assign to space-charge buildup above the ruthenium surface. This will require special consideration when designing future X-ray two-pulse correlation measurements.

## II. EXPERIMENTAL AND THEORETICAL METHODS

The experimental procedure is illustrated in Fig. 1. We used soft X-ray pulses generated at the Linac Coherent Light Source (LCLS) at SLAC National Accelerator Laboratory. The *fresh-slice* multi-pulse mode<sup>25</sup> provided pairs of two X-ray pulses (double pulses) or alternatively a single pulse at around 530 eV photon energy with 30 Hz repetition rate,  $\sim 1.5$  eV bandwidth, up to 500  $\mu\text{J}$  total (sum of the pair) pulse energy (10  $\mu\text{J}$  at the sample), and tunable delay of up to 950 fs

between the two pulses. We used single as well as 30 fs delayed double pulses. The pulse duration of individual pulses was  $\sim 4$  fs as determined from representative shots analyzed with the X-band radiofrequency transverse deflecting cavity (XTCAV).<sup>32</sup> Horizontal polarization of the X-rays was used, which is in plane with the sample surface.

The X-ray pulses irradiated the Ru(0001) surface under  $1.5^\circ$  grazing incidence. We used established surface science techniques to prepare a co-adsorbed phase of oxygen and CO on the Ru(0001) substrate with a (2O+CO)/Ru(0001) honeycomb surface structure ([supplementary material](#)). Prior to experiments at LCLS, the sample cleaning and overlayer preparation procedures were evaluated with synchrotron radiation-based X-ray photoelectron spectroscopy using the very same setup (see the [supplementary material](#)). The sample was cooled by liquid nitrogen to  $\sim 100$  K. To provide a fresh spot on the sample for each pulse pair, we continuously scanned the  $10 \times 10$  mm<sup>2</sup> substrate through the  $25 \times 70$   $\mu\text{m}^2$  X-ray beam ( $25 \times \sim 2700$   $\mu\text{m}^2$  footprint) at a speed of 0.8 mm/s. The sample was frequently cleaned to avoid any buildup of dissociated CO products using a procedure established during previous experiments at LCLS of CO on Ru where X-ray absorption spectroscopy was used with high sensitivity to atomic oxygen and none was detected.<sup>28</sup> CO and O<sub>2</sub> background pressure ensured readsorption of CO and oxygen onto the Ru(0001) surface during the time of one scan cycle, which enabled repetitive cycling over the sample.

We recorded the desorbing reaction products (mass 28 for CO or mass 44 for CO<sub>2</sub>) with a time-of-flight quadrupole mass spectrometer (Hiden Analytical) in a time window of 8 ms after the X-ray pulse (pair) hit the sample. Counts at a time-of-flight longer than 1.5 ms were used to determine the background count rate of the mass spectrometer. To determine the yield, the counts in the time-of-flight region between 0.1 and 1 ms were integrated after background subtraction and scaled by the relative mass spectrometer sensitivities for CO<sub>2</sub> and CO. The variation in X-ray fluence came from the intrinsic and, for XFEL typical, shot-to-shot intensity fluctuations ([supplementary material](#)).

Theoretical calculations were carried out using density functional theory (DFT). We model the surface by a periodic four-layer Ru slab with co-adsorbed O and CO and then use the GPAW code<sup>33,34</sup> to calculate potential energy surfaces of adsorbed O in the ground and core-excited states. To treat the valence-excited state, which results from Auger decay and subsequent screening, we use a Ru<sub>24</sub>O-cluster in the StoBe-deMon code.<sup>35</sup> The valence holes are modeled by constructing localized 2p-like orbitals on the atomic oxygen using occupied Kohn-Sham orbitals from a DFT ground state calculation. The occupation of these localized orbitals is then constrained to zero, and the rest of the electronic system is relaxed self-consistently with these orbitals frozen to find the lowest solution with this constraint. This treatment is similar to the linear-expansion delta-SCF method of Gavnholt *et al.*,<sup>36</sup> where electrons are confined to previously unoccupied orbitals; here we instead create holes in occupied orbitals. We note that this is a standard procedure in computing core-level binding energies using  $\Delta$ Kohn-Sham, which can also be

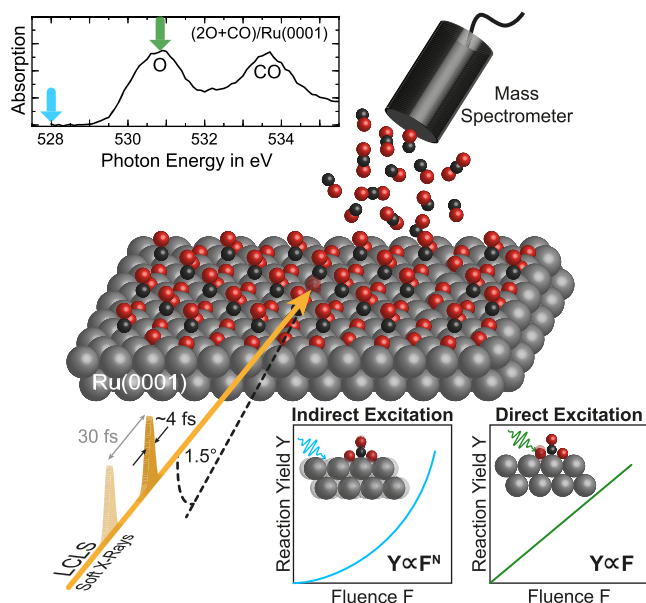


FIG. 1. Schematic illustration of the experimental procedure. Upper inset: oxygen  $1s$  X-ray absorption spectrum of co-adsorbed oxygen and CO on Ru(0001). Excitation energies used for yield measurements are indicated by arrows. Lower insets: schematic of the expected reaction-yield fluence-dependence for indirect excitation of the adsorbates via the substrate and direct excitation.

applied to variationally determine a sequence of orthogonal core-excited states.<sup>37,38</sup>

Further experimental and theoretical details are provided in the [supplementary material](#).

### III. RESULTS AND DISCUSSION

The X-rays incident onto the CO and oxygen covered ruthenium surface can induce a reaction of the adsorbates via several different mechanisms. For the discussion of our results, we divide these mechanisms into two classes: *substrate mediated* mechanisms, where the X-rays are initially absorbed by the ruthenium substrate, and *direct* mechanisms, where the X-rays are absorbed by the oxygen adsorbate.

For the former class, the X-rays are absorbed by the ruthenium substrate which results in hot electrons and phonons through processes that are intrinsically different from the direct single-electron photoexcitations into the conduction band that are typical of optical laser excitations. The X-rays, even at the extreme grazing incidence used here, penetrate several layers into the substrate and generate a multitude of photoelectrons from the ruthenium *3p* and *3d* levels and the valence band. The energy of the photoelectrons is sufficient for the electrons to leave the metal and not contribute to the substrate heating if emitted directly into vacuum; photoelectrons emitted from deeper layers will, however, undergo scattering due to the short mean free path in the metal and contribute to substrate heating. The Auger decay cascade in the substrate, which follows initial core level ionization, generates additional Auger electrons which will also scatter within the substrate as well as at surface adsorbates and lose part of their kinetic energy. This inelastic scattering within the substrate produces secondary electrons and ultimately results in a hot electron distribution in the substrate which in turn can excite substrate phonons. This results in a sharp rise in electronic and vibrational temperature of the substrate, and both the resulting hot electrons and phonons may couple to adsorbates and induce a reaction. For these substrate mediated processes, the reaction kinetics are determined by the X-ray induced temperature of substrate electrons and phonons. Although the complicated processes behind the X-ray heating of the substrate make it, in contrast to heating with an optical laser, difficult to reliably estimate the temperature, the reaction yield will follow either an Arrhenius-type or a power law expression when dominated by, respectively, the equilibrated phonon temperature or non-equilibrium hot-electron-mediated excitations of the adsorbate; both cases result in a non-linear increase with incident X-ray fluence as schematically depicted in the lower left inset in Fig. 1. The reaction yield dependence due to hot electrons can typically be parameterized by a power law of the form  $Y \propto F^N$  with yield  $Y$ , fluence  $F$ , and an exponent  $N$  typically ranging from three to eight.<sup>7,39</sup> Since this class of substrate-mediated mechanisms has been discussed in detail in connection to optical and infrared light excitations and is not the main focus of the present work, we refer the interested reader to the literature, e.g., Refs. 7, 27, 40–42. We note, however, that a non-linear fluence dependence can in principle also result from multiple direct excitations at the same adsorbate. With the low adsorbate excitation density achieved in

this work (see below), a substantial contribution from multiple excitations can, however, be excluded.

In the second class of reaction mechanisms, X-ray absorption directly excites the adsorbate via, e.g., core-level excitation. The accompanying changes in the adsorbate electronic structure and adsorbate-substrate bonding may provide sufficient energy to induce nuclear motion and subsequent reactions. For this direct excitation mechanism, each incident X-ray photon will trigger an adsorbate reaction with a certain probability and hence the reaction yield will be directly proportional to the number of incident photons and show a linear fluence dependence (Fig. 1, lower right inset).

We also note that substrate mediated processes can result in a linear fluence dependence, when, e.g., excited substrate electrons scatter at an adsorbate and induce single electronic adsorbate excitation. Such processes are discussed in the literature often under the term DIET (desorption induced by electronic transition) within the so-called GMR (Gomer-Menzel-Redhead) mechanism (see Refs. 43–46 and the references therein). These processes are, however, available both when exciting non-resonantly and resonantly with X-rays and thus do not contribute to differences between these two cases.

In Fig. 1 (upper left inset), we show the X-ray absorption spectrum of co-adsorbed CO and oxygen on Ru(0001) ([supplementary material](#)) around the oxygen *1s* resonance. The two resonances of atomically adsorbed oxygen at 530.8 eV and adsorbed CO at 533.6 eV are separated by a 2.8 eV chemical shift. Hence, the photon energy bandwidth used in our experiment of  $\sim 1.5$  eV allows us to excite the adsorbates separately. We recorded the CO<sub>2</sub> and CO yield as a function of total X-ray fluence using excitation energies of 528 eV, well below the oxygen *1s* resonance, and 530.8 eV coinciding with the atomic oxygen resonance. We limit the discussion to these two photon energies but show data for excitation on the CO resonance at 533.6 eV in the [supplementary material](#).

In Figs. 2(a)–2(d), we depict the yield of CO<sub>2</sub> and CO as a function of X-ray fluence on the sample after irradiation with single X-ray pulses of 528 eV and 530.8 eV photon energy. The yields have been background subtracted and scaled by the relative mass spectrometer sensitivities for CO<sub>2</sub> and CO. Hence, we can directly compare the yields for CO<sub>2</sub> and CO. Note the factor of ten difference in  $y$ -scale between the CO<sub>2</sub> and CO yields. For both photon energies, we measure a clear fluence-dependent CO<sub>2</sub> signal, which shows that the incident X-rays drive CO oxidation. CO desorption (CO yield) dominates over CO oxidation (CO<sub>2</sub> yield) for both photon energies. All yield curves show a non-linear increase with increasing fluence, but, as we analyze in detail below, with different non-linearity. The error bars are given as  $1\sigma$  in the counting statistics, where the largest uncertainty is for the data points at the upper fluence range. This is caused by the relatively large (as compared to the conventional self-amplified spontaneous emission (SASE) operation mode of the LCLS) intensity fluctuations with the *fresh-slice* multi-pulse mode that was used in the experiment. Therefore shots at the upper limit of the fluence range are relatively rare. The two points in Fig. 2(c) that appear at the negative yield are due to background subtraction which was applied to all data and is particularly important for CO due

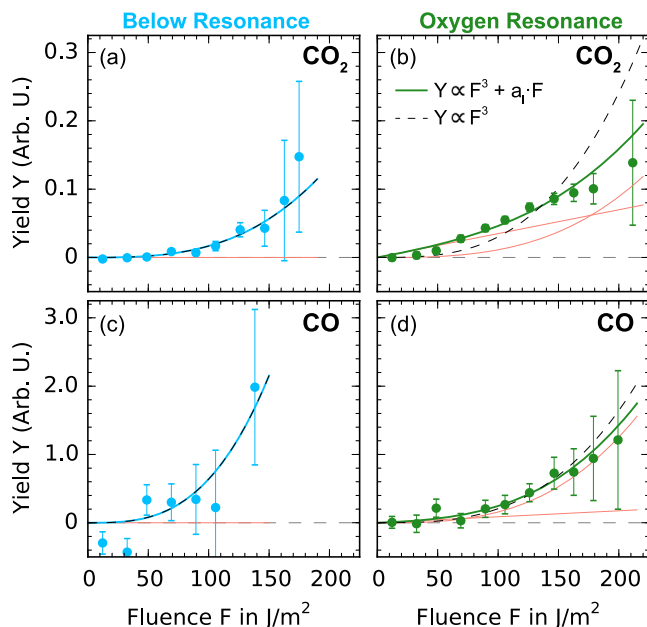


FIG. 2. CO<sub>2</sub> [(a) and (b)] and CO [(c) and (d)] yields as a function of X-ray fluence on the sample for incident photon energies of 528 eV [below resonance, (a) and (c)] and 530.8 eV [oxygen resonance, (b) and (d)] using single pulses. Markers represent measured data with 1 sigma counting statistics error bars. Dashed black lines as well as blue and green solid lines are fitted curves using power law as well as a linear plus power law. Red lines correspond to the individual linear and power law contributions (see the text for details). The legend in (b) is valid for all four panels.

to the background pressure but are still within  $3\sigma$  of positive yield values.

At excitation below resonance [Figs. 2(a) and 2(c)], the incident photons do not excite oxygen 1s core-level electrons but are exclusively absorbed (and partly reflected) by the ruthenium substrate. Hence, the observed CO oxidation and desorption must be driven by substrate mediated mechanisms. We follow the approach established for optical laser-driven surface reactions and model the fluence dependence with a power law  $Y = a_p F^N$ , with  $Y$  and  $F$  being the yield and fluence and  $a_p$  and  $N$  being the fitted amplitude and power law exponent. We find an exponent of  $N = 3.1$  for the CO<sub>2</sub> and CO yields (with uncertainties  $\pm 0.5$  for CO<sub>2</sub> and  $\pm 2.5$  for CO) at below resonance excitation. The CO<sub>2</sub>:CO yield ratio is around 1:35 independent of fluence. This exponent and yield ratio are identical within error bars to the values obtained with 800 nm laser excitation,<sup>42,47</sup> where CO oxidation and desorption were found to be substrate mediated and driven by hot substrate electrons (oxidation) and phonons (desorption). We note a seeming difference in substrate-mediated yields when exciting below and on resonance, but for the CO<sub>2</sub> yield [Figs. 2(a) and 2(b)], the amplitude of the fitted substrate-mediated component is  $(2.6 \pm 0.6) \times 10^{-7}$  and  $(1.7 \pm 0.5) \times 10^{-7}$  for Figs. 2(a) and 2(b), respectively, and hence they are identical within error bars. For the CO yield [Figs. 2(c) and 2(d)], the corresponding amplitudes are  $(10 \pm 11) \times 10^{-6}$  and  $(2.4 \pm 0.6) \times 10^{-6}$  for Figs. 2(c) and 2(d), respectively, but the large uncertainty in the fit in Fig. 2(c) makes a direct comparison more difficult.

At resonant oxygen 1s excitation, only about 0.1% of the incident photons are absorbed by adsorbed oxygen atoms

(supplementary material),<sup>48</sup> while the remaining photons are absorbed or reflected by the substrate. Hence, one could expect that also for resonant excitation the observed CO oxidation and desorption originate predominantly from substrate-mediated processes and can be described with a power law exponent of  $N \approx 3$  as found for non-resonant X-ray and 800 nm laser excitation. However, when fitting the fluence dependence at resonant excitation with the power law, we obtain exponents of  $N = 1.6 \pm 0.1$  for the CO<sub>2</sub> yield and  $N = 2.4 \pm 0.4$  for the CO yield (see Fig. S3 in the supplementary material). At the same time, constraining the exponent in the power law to  $N = 3$ , we find that it describes the CO yield well but fails to describe the CO<sub>2</sub> yield (see dashed lines in Fig. 2). On the other hand, adding a linear component to the power law to account for contributions from direct X-ray excitation and constraining the exponent to  $N = 3$  to account for contributions from substrate-mediated processes ( $Y = a_p F^3 + a_1 F$ ) results in a good representation of the CO and the CO<sub>2</sub> yields (solid lines in Fig. 2). From this extended model, we find a substantial linear component in the CO<sub>2</sub> yield at resonant excitation on top of the power law background. Applying the superposition of power law and linear component to the other fluence curves, we find a small linear component in the CO yield at resonant excitation (supplementary material), while below resonance both fluence curves are well represented solely by the power law. To confirm the statistical significance of a linear component in the CO<sub>2</sub> yield at resonant excitation, we performed statistical hypothesis testing, where details are provided in the supplementary material. The linear component in the fluence dependence of the CO<sub>2</sub> yield at resonant excitation strongly suggests that 1s core-level excitation of atomically adsorbed oxygen directly drives CO oxidation from co-adsorbed CO and oxygen on Ru(0001).

To understand how resonant 1s excitation can drive CO oxidation, we illustrate in the top part of Fig. 3 the main electronic states following the excitation. X-ray absorption promotes the oxygen atom into a core-excited state. The excited electron delocalizes on a femtosecond time scale<sup>49–52</sup> and thereby the core-excited state can be viewed as a core-hole state fully screened by the substrate. The core-hole state decays with  $\sim 4$  fs lifetime<sup>53</sup> predominantly via Auger decay resulting in a valence-excited state with two localized valence holes which are screened by charge transfer from the substrate. The resulting electronic state for the atomic oxygen can thus be described as doubly valence-excited.

To identify the driving electronic state for CO oxidation, we performed DFT calculations of the potential energy curves along the surface normal (supplementary material) of atomically adsorbed oxygen in the (2O+CO)/Ru(0001) phase. The calculated potential energy curves in Fig. 3(a) show that the core-excited oxygen is still bound to the surface with an equilibrium distance just about 0.25 Å larger than in the electronic ground state. The response of the valence electrons to screen the core hole gives rise to a fluorine-like electronic configuration,<sup>54</sup> which can be written as  $(1s^1)(2s^2)[2p^{4+1}]$  (see Fig. 3 for nomenclature), where core-excited oxygen and ground state fluorine give near-identical potential curves (supplementary material). Hence, the core-level excitation itself does not result in substantial activation of oxygen. For the valence-excited

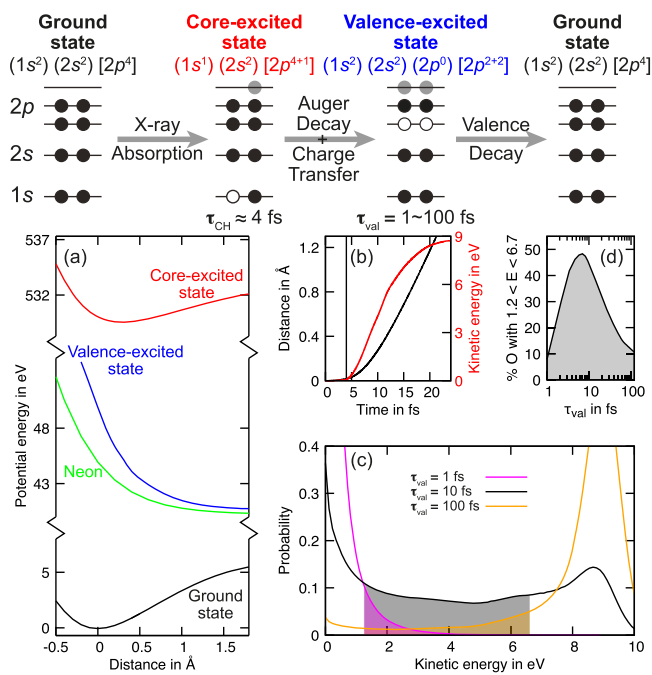


FIG. 3. Top panel: Schematic illustration of electronic states of adsorbed oxygen following  $1s$  excitation. Filled and open circles denote electrons and holes, and gray filled circles represent screening electrons. Note that due to ultrafast delocalization in the core-excited state this will result in a fully screened core-hole state on a subfemtosecond time scale. Rounded parentheses and square brackets in the electron configurations denote orbitals of strongly localized core-like character, respectively, valence type character. Lower panels (a)–(d): DFT results: (a) potential energy of atomic oxygen on Ru(0001) as a function of distance normal to the surface, relative to the ground state equilibrium distance for electronic ground, core-excited, and valence-excited states and of neon on Ru(0001). (b) Distance from the ground state equilibrium position and kinetic energy of oxygen as a function of time after oxygen  $1s$  ionization assuming  $\tau_{\text{CH}} = 4$  fs core-hole lifetime. (c) Distribution of final kinetic energies after the excited oxygen decays back into the electronic ground state assuming exponential decay of the core-excited state with 4 fs and of the valence excited state with  $\tau_{\text{val}} = 1, 10,$  and  $100$  fs lifetime. (d) Percentage of initially excited oxygen atoms that gain kinetic energy between  $1.2$  and  $6.7$  eV for which CO oxidation is energetically possible as a function of valence-excited state lifetime.

state, we limit the discussion to the  $2p^{-2}$  state with both holes in the oxygen  $2p$  level. This is the dominant Auger final state,<sup>55</sup> and other Auger final states show similar results (supplementary material). In this valence-excited Auger final state, the two valence holes are correlated and localized at the oxygen atom as observed in early studies of Auger electron spectra of adsorbed oxygen.<sup>55,56</sup> This localization isolates the valence holes and eliminates orbital mixing, similar to a core hole, which justifies our DFT treatment (supplementary material). At the same time, the localized valence holes are efficiently screened by filling the formerly unoccupied oxygen  $2p$  orbitals resulting in an effectively neutral Auger final state, interacting with the substrate as if it were closed-shell. The electron configuration in the Auger final state can hence be written as  $(1s^2)(2s^2)(2p^0)[2p^{2+2}]$ . This  $p$ -shell configuration for a neutral atom can be compared to the neon electronic closed-shell configuration, which explains the resemblance and strongly repulsive character of the potential curves of the oxygen Auger final state and ground state neon, as seen in Fig. 3(a). In an orbital picture, one can explain the strongly repulsive character of the Auger final state by the presence of holes in

the highest occupied oxygen orbital, which has a bonding character with respect to the O–Ru bond, and additional screening electrons in the lowest unoccupied oxygen orbital which has an anti-bonding character.

The repulsive potential in the valence-excited state causes the oxygen to increase its distance to the surface and gain kinetic energy [Fig. 3(b)]. The amount of kinetic energy gained by the valence-excited oxygen depends on the lifetime of this valence-excited state. Due to the efficient screening of the two valence holes as well as hole-hole correlation,<sup>8</sup> we can expect a relatively long valence-hole lifetime of a few and up to around  $100$  femtoseconds. If, by the time the valence-excited oxygen decays back into its electronic ground state, its kinetic energy exceeds the ground state binding energy to the ruthenium surface (calculated to be  $6.7$  eV), it will desorb from the surface. If, on the other hand, the decay into the ground state occurs early, the oxygen remains on the surface vibrationally “hot”. It will then redistribute its kinetic energy via inelastic scattering with substrate atoms and neighboring adsorbates into all degrees of freedom, which will also include the reaction coordinate for CO oxidation. For CO oxidation to be energetically possible, the kinetic energy gained in the valence-excited state needs to be larger than the reaction barrier for CO oxidation of  $1.2$  eV on Ru(0001)<sup>29</sup> and smaller than the binding energy to the ruthenium surface of  $6.7$  eV (see above).

The fraction of initially excited oxygen atoms that fall within the energy boundaries to enable CO oxidation ( $1.2$  eV  $< E_{\text{Kin}} < 6.7$  eV) is represented by the shaded areas in Fig. 3(c), where we have calculated the distribution of final kinetic energies assuming an exponentially decaying population of valence-excited oxygen atoms with three different lifetimes. From Fig. 3(d), we see that for the entire range of reasonable valence-excited state lifetimes ( $1$ – $100$  fs),  $10\%$  or more of initially excited oxygen atoms gain kinetic energy that makes CO oxidation energetically possible.

Hence, irrespective of its exact lifetime, the valence-excited state provides sufficient energy to a substantial number of excited oxygen atoms to overcome the reaction barrier toward CO oxidation. A fraction of these oxygen atoms will transfer their kinetic energy into the reaction coordinate to eventually react with a neighboring CO molecule and form  $\text{CO}_2$ . We therefore identify the valence-excited state of adsorbed oxygen as the driving state for CO oxidation after resonant oxygen  $1s$  excitation. This is consistent with early studies of X-ray induced desorption of adsorbate fragments and the GMR mechanism.<sup>8,18,19,43–45,57</sup>

Two-pulse correlation (2PC) measurements using optical laser pulses have been reported earlier and used to discriminate between hot-electron-driven and thermally activated oxidation of CO on Ru(0001).<sup>42,47</sup> Here we exploit the availability of the novel double-pulse scheme to explore the feasibility of 2PC measurements in the X-ray regime. A target for future experiments with variable pulse separation would, e.g., be a direct determination of the lifetime of the double valence-hole state. In the present exploratory study, only a fixed separation of  $30$  fs could be used (due to limited experimental time and not a technical limitation) which we report since it reveals some challenges with this approach.

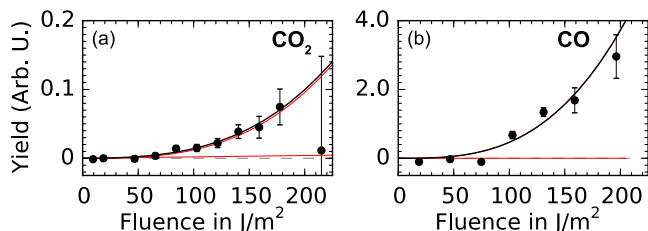


FIG. 4. CO<sub>2</sub> (a) and CO (b) yield as a function of total X-ray fluence on the sample using double pulses with 30 fs delay and both tuned to the atomic oxygen resonance. For markers and line style description, see Fig. 2.

In Fig. 4, we depict the CO<sub>2</sub> and CO yields as a function of total fluence using the 30 fs delayed double pulse and also show that with the double-pulses we drive CO oxidation. Fitting the double-pulse fluence dependence with the superposition of linear and power law ( $Y = a_p F^3 + a_l F$ ) reveals that the non-linear power-law component is significantly stronger for the double pulse as compared to the single pulse (compare Figs. 2 and 4). Hence, the substrate-mediated contribution to the total reaction yield seems to be enhanced with the double pulse which complicates the use of this technique since it implies a change in reaction mechanism with the second pulse.

We tentatively assign the origin of the enhanced contribution of substrate-mediated processes to well-known space charge effects<sup>58</sup> where the photoelectrons emitted by the first pulse remain as a space charge cloud in the vicinity of the sample and reduce the possibility for photoelectrons of the second pulse to escape into vacuum<sup>59</sup> and thus a larger fraction of the emitted electrons will deposit their energy in the substrate. The formation time of this space charge cloud is likely on the few-femtosecond time scale and thus comparable to the X-ray pulse duration. Its lifetime, on the other hand, is on the order of pico- to nano-seconds.<sup>60,61</sup> The space charge cloud will be present for a single pulse as well as double pulses, but since the formation time of the space charge cloud is comparable to the X-ray pulse duration, we can expect its impact to be smaller for the single pulse. Hence, we can also expect the electronic and vibrational temperatures of the substrate to increase more with the double pulse with 30 fs delay as compared to the single pulse at a similar total fluence which may explain the enhanced contribution of substrate-mediated mechanisms to the total reaction yield. The observed heating effect, whether due to the here proposed formation of a space charge cloud as a lid over the substrate or of a different origin, clearly needs to be taken into account when planning future 2PC X-ray measurements, but using even shorter X-ray pulses and a variable delay may also provide opportunities to investigate this effect in detail.

#### IV. SUMMARY

In summary, we have shown how resonant oxygen 1s excitation of atomic oxygen in co-adsorbed CO and oxygen on Ru(0001) selectively activates the oxygen and drives CO oxidation. Our DFT calculations show that the strongly repulsive potential for the valence-excited oxygen on Ru(0001) that follows Auger decay and stems from holes in bonding and

additional screening electrons in anti-bonding orbitals is the driving force for oxygen activation and eventually CO oxidation. Using the multi-pulse scheme of the LCLS to drive CO oxidation, we investigate the prospects of the femtosecond X-ray pump X-ray spectroscopy probe and X-ray two-pulse correlation to study the reaction path, dynamics, and underlying electronic structure modifications of atom-specifically activated chemical reactions. We find complications with two-pulse correlation studies in the X-ray regime due to enhanced heating effects, but envision broad application of these techniques for fundamental investigations of reaction mechanisms, and chemical selectivity in general, via selective X-ray excitation.

#### SUPPLEMENTARY MATERIAL

In the [supplementary material](#), we present further experimental details, CO resonance fluence dependence, calculation of the fraction of excited adsorbates, and details on the DFT calculations.

#### ACKNOWLEDGMENTS

We acknowledge funding from the Knut and Alice Wallenberg Foundation and the Swedish Research Council. Portions of this research were carried out on the SXR Instrument at the Linac Coherent Light Source (LCLS), a division of SLAC National Accelerator Laboratory and an Office of Science user facility operated by Stanford University for the U.S. Department of Energy. The SXR Instrument is funded by a consortium whose membership includes the LCLS, Stanford University through the Stanford Institute for Materials Energy Sciences (SIMES), Lawrence Berkeley National Laboratory (LBNL), the University of Hamburg through BMBF priority Program No. FSP 301, and the Center for Free Electron Laser Science (CFEL). The LCLS is funded by the DOE Office of Basic Energy Sciences. This work was in part supported by the U.S. Department of Energy, Laboratory Directed Research and Development funding, under Contract No. DE-AC02-76SF00515. The DFT calculations were performed using computational resources provided by the Swedish National Infrastructure for Computing (SNIC) at the HPC2N center. Furthermore this work was funded in parts by the Volkswagen Stiftung.

<sup>1</sup>J. K. Nørskov, T. Bligaard, A. Logadottir, S. Bahn, L. B. Hansen, M. Bollinger, H. Bengaard, B. Hammer, Z. Sljivancanin, M. Mavrikakis, Y. Xu, S. Dahl, and C. J. H. Jacobsen, *J. Catal.* **209**, 275 (2002).

<sup>2</sup>T. Bligaard, J. K. Nørskov, S. Dahl, J. Matthiesen, C. H. Christensen, and J. Sehested, *J. Catal.* **224**, 206 (2004).

<sup>3</sup>F. Abild-Pedersen, J. Greeley, F. Studt, J. Rossmeisl, T. R. Munter, P. G. Moses, E. Skúlason, T. Bligaard, and J. K. Nørskov, *Phys. Rev. Lett.* **99**, 016105 (2007).

<sup>4</sup>L. C. Grabow, B. Hvolbæk, and J. K. Nørskov, *Top. Catal.* **53**, 298 (2010).

<sup>5</sup>A. J. Medford, A. Vojvodic, J. S. Hummelshøj, J. Voss, F. Abild-Pedersen, F. Studt, T. Bligaard, A. Nilsson, and J. K. Nørskov, *J. Catal.* **328**, 36 (2015).

<sup>6</sup>X.-L. Zhou, X.-Y. Zhu, and J. M. White, *Surf. Sci. Rep.* **13**, 73 (1991).

<sup>7</sup>C. Frischkorn and M. Wolf, *Chem. Rev.* **106**, 4207 (2006).

<sup>8</sup>D. Menzel, *J. Chem. Phys.* **137**, 091702 (2012).

<sup>9</sup>K. Watanabe, K. Sawabe, and Y. Matsumoto, *Phys. Rev. Lett.* **76**, 1751 (1996).

- <sup>10</sup>M. Wolf, A. Hotzel, E. Knoesel, and D. Velic, *Phys. Rev. B* **59**, 5926 (1999).
- <sup>11</sup>H. Petek, M. J. Weida, H. Nagano, and S. Ogawa, *Science* **288**, 1402 (2000).
- <sup>12</sup>H. Petek and S. Ogawa, *Annu. Rev. Phys. Chem.* **53**, 507 (2002).
- <sup>13</sup>H. Petek, *J. Chem. Phys.* **137**, 091704 (2012).
- <sup>14</sup>Y. Suchorski, N. Ernst, W. a. Schmidt, V. K. Medvedev, H. J. Kreuzer, and R. L. C. Wang, *Prog. Surf. Sci.* **53**, 135 (1996).
- <sup>15</sup>J. H. Block, D. L. Cocke, and N. Kruse, in *Handbook of Heterogeneous Catalysis*, edited by G. Ertl, H. Knözinger, and J. Weitkamp (VCH Verlagsgesellschaft mbH, 1997), pp. 1104–1123.
- <sup>16</sup>A. Huzayyin, J. H. Chang, K. Lian, and F. Dawson, *J. Phys. Chem. C* **118**, 3459 (2014).
- <sup>17</sup>J. L. LaRue, T. Katayama, A. Lindenberg, A. S. Fisher, H. Öström, A. Nilsson, and H. Ogasawara, *Phys. Rev. Lett.* **115**, 036103 (2015).
- <sup>18</sup>R. Jaeger, J. Stöhr, R. Treichler, and K. Baberschke, *Phys. Rev. Lett.* **47**, 1300 (1981).
- <sup>19</sup>S. P. Frigo, P. Feulner, B. Kassühlke, C. Keller, and D. Menzel, *Phys. Rev. Lett.* **80**, 2813 (1998).
- <sup>20</sup>K. Tanaka, E. O. Sako, E. Ikenaga, K. Isari, S. A. Sardar, S. Wada, T. Sekitani, K. Mase, and N. Ueno, *J. Electron Spectrosc. Relat. Phenom.* **119**, 255 (2001).
- <sup>21</sup>A. A. Lutman, R. Coffee, Y. Ding, Z. Huang, J. Krzywinski, T. Maxwell, M. Messerschmidt, and H.-D. Nuhn, *Phys. Rev. Lett.* **110**, 134801 (2013).
- <sup>22</sup>A. Marinelli, A. A. Lutman, J. Wu, Y. Ding, J. Krzywinski, H.-D. Nuhn, Y. Feng, R. N. Coffee, and C. Pellegrini, *Phys. Rev. Lett.* **111**, 134801 (2013).
- <sup>23</sup>A. Marinelli, D. Ratner, A. A. Lutman, J. Turner, J. Welch, F.-J. Decker, H. Loos, C. Behrens, S. Gilevich, A. A. Miahnahri, S. Vetter, T. J. Maxwell, Y. Ding, R. Coffee, S. Wakatsuki, and Z. Huang, *Nat. Commun.* **6**, 6369 (2015).
- <sup>24</sup>A. A. Lutman, F. J. Decker, J. Arthur, M. Chollet, Y. Feng, J. Hastings, Z. Huang, H. Lemke, H. D. Nuhn, A. Marinelli, J. L. Turner, S. Wakatsuki, J. Welch, and D. Zhu, *Phys. Rev. Lett.* **113**, 254801 (2014).
- <sup>25</sup>A. A. Lutman, T. J. Maxwell, J. P. MacArthur, M. W. Guetg, N. Berrah, R. N. Coffee, Y. Ding, Z. Huang, A. Marinelli, S. Moeller, and J. C. U. Zemella, *Nat. Photonics* **10**, 745 (2016).
- <sup>26</sup>F. Budde, T. F. Heinz, M. M. T. Loy, J. A. Misewich, F. de Rougemont, and H. Zacharias, *Phys. Rev. Lett.* **66**, 3024 (1991).
- <sup>27</sup>C. Hess, S. Funk, M. Bonn, D. N. Denzler, M. Wolf, and G. Ertl, *Appl. Phys. A: Mater. Sci. Process.* **71**, 477 (2000).
- <sup>28</sup>M. Dell'Angela, T. Anniyev, M. Beye, R. Coffee, A. Föhlisch, J. Gladh, T. Katayama, S. Kaya, O. Krupin, J. LaRue, A. Møgelhøj, D. Nordlund, J. K. Nørskov, H. Öberg, H. Ogasawara, H. Öström, L. G. M. Pettersson, W. F. Schlotter, J. A. Sellberg, F. Sorgenfrei, J. J. Turner, M. Wolf, W. Wurth, and A. Nilsson, *Science* **339**, 1302 (2013).
- <sup>29</sup>H. Öström, H. Öberg, H. Xin, J. LaRue, M. Beye, M. Dell'Angela, J. Gladh, M. L. Ng, J. A. Sellberg, S. Kaya, G. Mercurio, D. Nordlund, M. Hantschmann, F. Hieke, D. Kühn, W. F. Schlotter, G. L. Dakovski, J. J. Turner, M. P. Miniti, A. Mitra, S. P. Moeller, A. Föhlisch, M. Wolf, W. Wurth, M. Persson, J. K. Nørskov, F. Abild-Pedersen, H. Ogasawara, L. G. M. Pettersson, and A. Nilsson, *Science* **347**, 978 (2015).
- <sup>30</sup>M. Beye, H. Öberg, H. Xin, G. L. Dakovski, M. Dell'Angela, A. Föhlisch, J. Gladh, M. Hantschmann, F. Hieke, S. Kaya, D. Kühn, J. LaRue, G. Mercurio, M. P. Miniti, A. Mitra, S. P. Moeller, M. L. Ng, A. Nilsson, D. Nordlund, J. Nørskov, H. Öström, H. Ogasawara, M. Persson, W. F. Schlotter, J. A. Sellberg, M. Wolf, F. Abild-Pedersen, L. G. M. Pettersson, and W. Wurth, *J. Phys. Chem. Lett.* **7**, 3647 (2016).
- <sup>31</sup>A. Nilsson, J. LaRue, H. Öberg, H. Ogasawara, M. Dell'Angela, M. Beye, H. Öström, J. Gladh, J. K. Nørskov, W. Wurth, F. Abild-Pedersen, and L. G. M. Pettersson, *Chem. Phys. Lett.* **675**, 145 (2017).
- <sup>32</sup>C. Behrens, F.-J. Decker, Y. Ding, V. A. Dolgashov, J. Frisch, Z. Huang, P. Krejčík, H. Loos, A. Lutman, T. J. Maxwell, J. Turner, J. Wang, M.-H. Wang, J. Welch, and J. Wu, *Nat. Commun.* **5**, 3762 (2014).
- <sup>33</sup>J. J. Mortensen, L. B. Hansen, and K. W. Jacobsen, *Phys. Rev. B* **71**, 035109 (2005).
- <sup>34</sup>J. Enkovaara, C. Rostgaard, J. J. Mortensen, J. Chen, M. Dulak, L. Ferrighi, J. Gavnholt, C. Glinsvad, V. Haikola, H. A. Hansen, H. H. Kristoffersen, M. Kuisma, A. H. Larsen, L. Lehtovaara, M. Ljungberg, O. Lopez-Acevedo, P. G. Moses, J. Ojanen, T. Olsen, V. Petzold, N. A. Romero, J. Stausholm-Møller, M. Strange, G. A. Tritsarlis, M. Vanin, M. Walter, B. Hammer, H. Häkkinen, G. K. H. Madsen, R. M. Nieminen, J. K. Nørskov, M. Puska, T. T. Rantala, J. Schiøtz, K. S. Thygesen, and K. W. Jacobsen, *J. Phys.: Condens. Matter* **22**, 253202 (2010).
- <sup>35</sup>K. Hermann, L. G. M. Pettersson, M. E. Casida, C. Daul, A. Goursot, A. Koester, E. Proynov, A. St-Amant, and D. R. Salahub, “StoBe-deMon” Program Version 3.3 (2014), available at <http://www.fhi-berlin.mpg.de/KHsoftware/StoBe/>.
- <sup>36</sup>J. Gavnholt, T. Olsen, M. Engelund, and J. Schiøtz, *Phys. Rev. B* **78**, 075441 (2008).
- <sup>37</sup>C. Kolczewski, R. Püttner, O. Plashkevych, H. Ågren, V. Staemmler, M. Martins, G. Snell, A. S. Schlachter, M. Sant'Anna, G. Kaindl, and L. G. M. Pettersson, *J. Chem. Phys.* **115**, 6426 (2001).
- <sup>38</sup>M. Leetmaa, M. P. Ljungberg, A. Lyubartsev, A. Nilsson, and L. G. M. Pettersson, *J. Electron Spectrosc. Relat. Phenom.* **177**, 135 (2010).
- <sup>39</sup>T. Olsen and J. Schiøtz, *Phys. Rev. Lett.* **103**, 238301 (2009).
- <sup>40</sup>R. R. Cavanagh, D. S. King, J. C. Stephenson, and T. F. Heinz, *J. Phys. Chem.* **97**, 786 (1993).
- <sup>41</sup>D. G. Busch and W. Ho, *Phys. Rev. Lett.* **77**, 1338 (1996).
- <sup>42</sup>M. Bonn, S. Funk, C. Hess, D. N. Denzler, C. Stampfl, M. Scheffler, M. Wolf, and G. Ertl, *Science* **285**, 1042 (1999).
- <sup>43</sup>D. Menzel and R. Gomer, *J. Chem. Phys.* **40**, 1164 (1964).
- <sup>44</sup>D. Menzel and R. Gomer, *J. Chem. Phys.* **41**, 3311 (1964).
- <sup>45</sup>P. A. Redhead, *Can. J. Phys.* **42**, 886 (1964).
- <sup>46</sup>D. Menzel, *Nucl. Instrum. Methods Phys. Res., Sect. B* **101**, 1 (1995).
- <sup>47</sup>H. Öberg, J. Gladh, K. Marks, H. Ogasawara, A. Nilsson, L. G. M. Pettersson, and H. Öström, *J. Chem. Phys.* **143**, 074701 (2015).
- <sup>48</sup>B. L. Henke, E. Gullikson, and J. C. Davis, *At. Data Nucl. Data Tables* **54**, 181 (1993).
- <sup>49</sup>E. Knoesel, T. Hertel, M. Wolf, and G. Ertl, *Chem. Phys. Lett.* **240**, 409 (1995).
- <sup>50</sup>R. M. Jaeger, K. Homann, H. Kühlenbeck, and H. J. Freund, *Chem. Phys. Lett.* **203**, 41 (1993).
- <sup>51</sup>O. Björneholm, A. Nilsson, A. Sandell, B. Hernnäs, and N. Mårtensson, *Phys. Rev. Lett.* **68**, 1892 (1992).
- <sup>52</sup>A. Föhlisch, P. Feulner, F. Hennies, A. Fink, D. Menzel, D. Sanchez-Portal, P. M. Echenique, and W. Wurth, *Nature* **436**, 373 (2005).
- <sup>53</sup>F. Gel'mukhanov, H. Ågren, M. Neeb, J.-E. Rubensson, and A. Bringer, *Phys. Lett. A* **211**, 101 (1996).
- <sup>54</sup>N. Mårtensson and A. Nilsson, *J. Electron Spectrosc. Relat. Phenom.* **75**, 209 (1995).
- <sup>55</sup>A. Sandell, A. Nilsson, O. Björneholm, H. Tillborg, and N. Mårtensson, *Phys. Rev. B* **48**, 11347 (1993).
- <sup>56</sup>J. C. Fuggle, E. Umbach, R. Kakoschke, and D. Menzel, *J. Electron Spectrosc. Relat. Phenom.* **26**, 111 (1982).
- <sup>57</sup>M. L. Knotek and P. J. Feibelman, *Phys. Rev. Lett.* **40**, 964 (1978).
- <sup>58</sup>J. P. Barbour, W. W. Dolan, J. K. Trolan, E. E. Martin, and W. P. Dyke, *Phys. Rev.* **92**, 45 (1953).
- <sup>59</sup>W. Wendelen, D. Auriq, and A. Bogaerts, *Appl. Phys. Lett.* **96**, 051121 (2010).
- <sup>60</sup>S. Hellmann, K. Rosnagel, M. Marczyński-Bühlow, and L. Kipp, *Phys. Rev. B* **79**, 035402 (2009).
- <sup>61</sup>M. Dell'Angela, T. Anniyev, M. Beye, R. Coffee, A. Föhlisch, J. Gladh, S. Kaya, T. Katayama, O. Krupin, A. Nilsson, D. Nordlund, W. F. Schlotter, J. A. Sellberg, F. Sorgenfrei, J. J. Turner, H. Öström, H. Ogasawara, M. Wolf, and W. Wurth, *Struct. Dyn.* **2**, 025101 (2015).